Monitoring the skin structure during edema *in vivo* with spatially resolved diffuse reflectance spectroscopy

Denis A. Davydov,[a,b,c] **Gleb S. Budylin**,[b,d] **Alexey V. Baev**,[a,d] **Daniil V. Vaypan**,[c] **Elena M. Seredenina**,[c] **Simon T. Matskeplishvili**,[c] **Stanislav A. Evlashin**,[e,*] **Armais A. Kamalov**,[c] **and Evgeny A. Shirshin**[a,b,*]

[a]Lomonosov Moscow State University, Faculty of Physics, Moscow, Russia
[b]First Moscow State Medical University, Biomedical Science and Technology Park, Laboratory of Clinical Biophotonics, Moscow, Russia
[c]Moscow State University, Medical Research and Education Center, Moscow, Russia
[d]Institute of Spectroscopy of the Russian Academy of Sciences, Moscow, Russia
[e]Skolkovo Institute of Science and Technology, Center for Materials Technologies, Moscow, Russia

Abstract

Significance: Edema occurs in the course of various skin diseases. It manifests itself in changes in water concentrations in skin layers: dermis and hypodermis and their thicknesses. In medicine and cosmetology, objective tools are required to assess the skin's physiological parameters. The dynamics of edema and the skin of healthy volunteers were studied using spatially resolved diffuse reflectance spectroscopy (DRS) in conjunction with ultrasound (US).

Aim: In this work, we have developed a method based on DRS with a spatial resolution (SR DRS), allowing us to simultaneously assess water content in the dermis, dermal thickness, and hypodermal thickness.

Approach: An experimental investigation of histamine included edema using SR DRS under the control of US was conducted. An approach for skin parameter determination was studied and confirmed using Monte-Carlo simulation of diffuse reflectance spectra for a three-layered system with the varying dermis and hypodermis parameters.

Results: It was shown that an interfiber distance of 1 mm yields a minimal relative error of water content determination in the dermis equal to 9.3%. The lowest error of hypodermal thickness estimation was achieved with the interfiber distance of 10 mm. Dermal thickness for a group of volunteers (7 participants, 21 measurement sites) was determined using SR DRS technique with an 8.3% error using machine learning approaches, taking measurements at multiple interfiber distances into account. Hypodermis thickness was determined with root mean squared error of 0.56 mm for the same group.

Conclusions: This study demonstrates that measurement of the skin diffuse reflectance response at multiple distances makes it possible to determine the main parameters of the skin and will serve as the basis for the development and verification of an approach that works in a wide range of skin structure parameters.

 [DOI: 10.1117/1.JBO.28.5.057002]

Keywords: spatially resolved diffuse reflectance spectroscopy; water in the skin; dermal thickness; hypodermal thickness; cutaneous edema.

Paper 220261GRR received Nov. 10, 2022; revised manuscript received Apr. 5, 2023; accepted for publication Apr. 5, 2023; published online May 13, 2023.

*Address all correspondence to Evgeny A. Shirshin, eshirshin@gmail.com; Stanislav A. Evlashin, s.evlashin@skoltech.ru

1 Introduction

The impaired balance of water distribution in the human organism accompanies numerous pathological states, and measuring water content in tissues is required for biomedical diagnostics. For instance, during heart failure,[1] physical examination using the "pitting scale" and weighing the patient remains the most useful approaches for assessing edematous syndrome; however, these methods are subjective and insufficient.[2] Assessment of water and lipids content in breast cancer tissues can provide important information about the characteristics of a tumor,[3] as the high water content in a tumor indicates edema and increased cellularity.[4,5] Likewise, the measurement of hydration in different skin layers is interesting for dermatology and cosmetology:[6] for instance, water content in the dermis is a marker of changes in the elastic properties of the skin,[7] and hydration of the stratum corneum is indicative of its barrier function.[8] Hence, the necessity of water content assessment stimulates the development of appropriate techniques, including those based on optical spectroscopy.[9]

Optical methods based on molecular contrast, i.e., spectroscopic signatures of water molecules, have been numerously suggested in the literature as fast, sensitive, and non-invasive tools for assessing hydration *in vivo*. Confocal Raman and THz spectroscopy are mainly applied for studying the skin's upper (epidermis) layer.[10,11] Near infrared (NIR) spectroscopy and imaging allow water content assessment in deeper layers (dermis and hypodermis).[3,12,13] For instance, in heart failure patients, peripheral edema was analyzed with short-wave NIR imaging.[2] Cutaneous edema induced by histamine application was studied with diffuse reflectance spectroscopy (DRS),[9,14] Raman fiber probe,[9] and multispectral NIR imaging.[2,9,15] The question of choosing the optimal distances between the source and the detector for leg edema evaluation were discussed in Nanjo et al.[14]

Since the optical and morphological properties of the skin differ significantly,[16] the assessment of hydration and cutaneous edema of the skin by optical methods is a complicated task. The top layer of the skin is the epidermis, 50 to 100 μm thick. Under the epidermis, there is the dermal layer, 1 to 2 mm thick. Dermis is mainly composed of collagen, which, along with elastic fibers, forms the extracellular matrix responsible for the viscoelastic properties of the skin.[17] Dermis contains blood capillaries; increased capillary permeability, e.g., during inflammation or heart failure, may result in interstitial fluid retention.[18] Below the dermis is the hypodermis, or the subcutaneous layer, which consists primarily of the fat tissue. There is a layer of muscle under the hypodermis. Its optical properties differ significantly from those of the hypodermis due to the higher water concentration and the absence of lipids in which the CH absorption band is more pronounced. The difference in the optical properties of the layers makes it possible to separate their contribution to the reflectance signal using spatially resolved DRS. Hence, when measuring the diffusely reflected NIR signal from the skin, water in the dermis and lipids in the hypodermis contribute to the spectrum. In this paper, we aim to simultaneously determine the molecular (water content in the dermis and lipid content in the hypodermis) and morphological (thickness of the dermis and hypodermis) properties of the skin (Fig. 1) *in vivo* using the spatially resolved DRS (SR DRS).

SR DRS is based on measuring spectra at varying source-detector distances, thus performing the depth scanning of a material.[19] To solve the inverse problem, i.e., to determine the absorption parameters from SR DRS data, Monte Carlo modeling of light propagation in multi-layered materials followed by interpolation[20,21] and machine learning[22–24] can be used. This approach has already proven itself capable of determining the content of hemoglobin and melanin in tissues. However, the problem of determining water *in vivo* using this technique has not been considered previously. The SR DRS has also been applied for determining the thicknesses of tissue layers in *ex vivo* samples and optical phantoms[12,25,26] thus making it a promising technique for sensing the properties of individual skin layers *in vivo*. This issue was also addressed in the present study.

Here, based on simulated and experimentally obtained SR DRS data, changes in water concentration and dermal and hypodermal layer thickness were investigated for the cases of cutaneous edema and normal skin. For calibration of parameters recovered from the DRS data, the thickness of the skin layers was measured by ultrasound (US) examination. The ability of the SR DRS to determine molecular and morphological parameters of the skin was evaluated

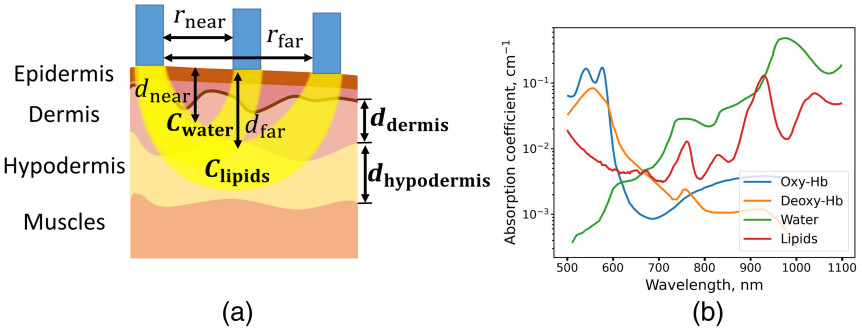

Fig. 1 (a) Schematic representation of the SR DRS method for the skin measurements *in vivo* and main parameters determining the optical response: water concentration in the dermis c_{water}, dermal thickness d_{dermis}, lipids content in the hypodermis c_{lipids}, and hypodermal thickness $d_{hypodermis}$. (b) Absorption spectra of the main skin chromophores: hemoglobin (Deoxy-Hb), oxyhemoglobin (Oxy-Hb), water, and lipids.

experimentally. The presented study is an important step for the development of a fully optical technique that can be useful for fluid retention estimation, pathological skin conditions, and dehydration assessment. Examination of skin physiology in cosmetology and dermatology may benefit from this approach.

2 Materials and Methods

2.1 *Diffuse Reflectance Spectra Measurement*

The setup used in this work allowed SR DRS measurement in the 400- to 1100-nm wavelength range using optical fibers with a core diameter of 550 μm. The photo of the experimental setup is presented in Fig. 2(a), while the photo and scheme of the DRS probe are presented in Figs. 2(b) and 2(c). The distance between the fibers was varied using a linear translation stage with a resonant piezoelectric motor (ELL17/M Stage, Thorlabs, United States) in the range from 0 to 10 mm with a 0.5-mm step and positioning accuracy of 50 μm. Detection was performed with a Maya2000Pro spectrometer (Ocean Optics, United States), and the SLS201 (Thorlabs, United States) was used as the light source. The effective optical density (OD) spectrum was calculated as follows:

$$\mathrm{OD}(\lambda) = -\ln\left(\frac{I(\lambda) - I_{bg}(\lambda)}{I_{\mathrm{ref}}(\lambda) - I_{bg}(\lambda)}\right), \tag{1}$$

where $I(\lambda)$ is the signal intensity of the sample, $I_{bg}(\lambda)$ is the background signal, and $I_{\mathrm{ref}}(\lambda)$ is the signal intensity from the reference sample (LabSphere, United States). Representative DRS spectra measured at different distances between the source and detector fibers are shown in Fig. 2(d). The optical fibers were located perpendicular to the skin surface in all experiments.

2.2 *Processing of Diffuse Reflection Spectra*

The OD spectra were fitted by a linear combination of the absorption spectra of the main components (water and lipids) and the baseline, which takes into account the contribution of the absorption of other chromophores (oxyhemoglobin, deoxyhemoglobin) and scattering:[9,27,28]

$$\mathrm{OD}(\lambda) = \mathrm{C}_0 + \mathrm{C}_1\lambda + A_{\mathrm{water}}\varepsilon_{\mathrm{water}}(\lambda) + A_{\mathrm{lipid}}\varepsilon_{\mathrm{lipid}}(\lambda), \tag{2}$$

where λ is the wavelength, C_0 and C_1 are related to contributions of background absorption and the scattering, A_{water} and A_{lipid} are the contributions of water and lipids absorption, $\varepsilon_{\mathrm{water}}(\lambda)$ and $\varepsilon_{\mathrm{lipid}}(\lambda)$ are the normalized absorption spectra of water and lipids. The coefficients were obtained

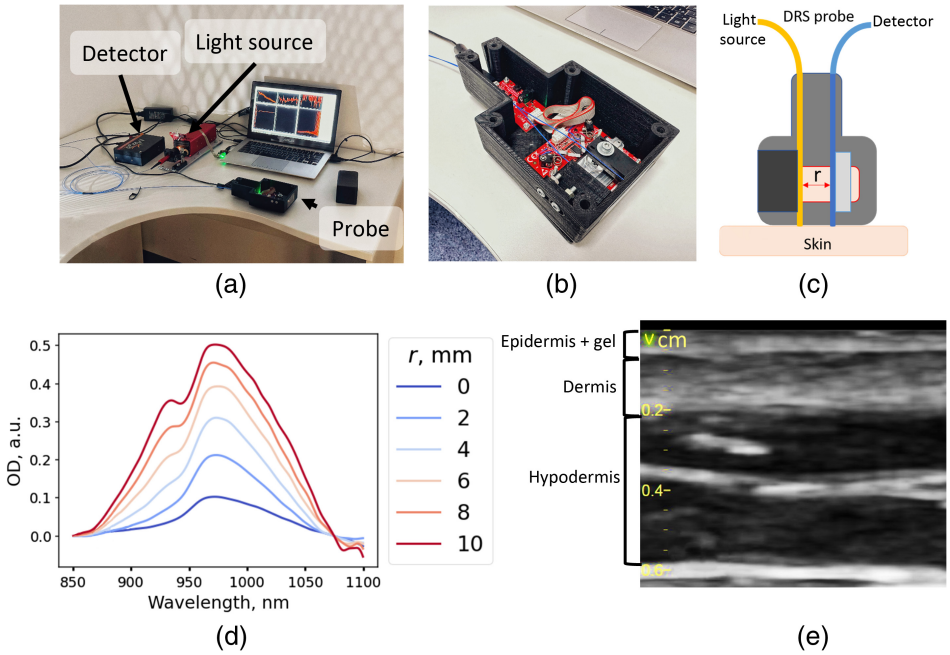

Fig. 2 Images and schematic of the setup and a typical view of the experimental data. (a) Photo of the experimental setup, (b) photo of the SR DRS probe, (c) the scheme of the SR DRS probe, (d) representative diffuse reflectance spectra measured for distances between the source and the detector in the range from 0 to 10 mm, and (e) US images of the skin obtained with a linear 11L-D probe at a scanning frequency of 12 MHz using the Vivid E95 device.

by minimizing the difference between the fitted and experimental spectra using the least squares method.

2.3 *Ultrasound Examination of the Skin*

Variations in the thickness of the skin layers during edema were investigated using the Vivid E95 device (GE Healthcare, United States) with a linear 11L-D probe at a scanning frequency of 12 MHz. The skin images obtained using the US examination allowed the determination of the thickness of the dermis and hypodermis [Fig. 2(e)]. The measurements were taken for at least five vertical profiles for each image using the ImageJ software.[29]

2.4 *Monte Carlo Simulation of Diffuse Reflectance Spectra*

Light propagation in the skin was simulated using the GPU implementation of the Monte Carlo Method [Monte Carlo modeling of light transport (MCML)].[30] The skin was modeled as a structure consisting of three layers with individual scattering and absorption properties. The first layer represented the dermis (where the water molecules are the main absorbers), the second layer simulated the hypodermis (with the lipids as the main absorber), and the third layer modeled the muscles (with the water as the main absorber). Using the simulation data, models were built to determine the water concentration in the dermis and the thickness of the dermis, as well as the thickness of the hypodermis. The determination of the parameters of the muscle layer was not carried out in the framework of this work.

The simulation was performed for varying values of the first d_{dermis} and second $d_{\text{hypodermis}}$ layer thicknesses and absorption coefficients of all layers: μ_{a1}, μ_{a2}, and μ_{a3}. The scattering coefficients of all layers were fixed to reduce the time required for simulations. The diffuse reflection coefficient R for each set of parameters was calculated as the ratio of the number of photon packets collected from the round-shaped region simulating an optical fiber with a diameter of 550 μm, exiting from the medium at all angles (solid angle of 2π steradian), to the number of photon packets entering the medium. For comparison, calculations were performed taking into

account the finite numerical aperture of the fiber (data not shown), the dependences that were obtained for the simulated data did not change qualitatively [see Figures S1(a) and S1(b) in the Supplementary Material]. Effective OD for the simulated data was calculated as $\mathrm{OD} = -\ln(R)$.[19] The distance between the detector and light source varied in the range from 0.025 to 15 mm with a step of 0.05 mm. Thus, simulation distance range was wider than the range in experiment. For each layer, the value of the absorption coefficient μ_{ai} ($i = 1,2,3$) varied in the range from 0.001 to 10 cm^{-1} on a logarithmic grid with 20 nodes. Scattering spectra for all layers were assumed to be independent of wavelength in the considered simulation range. The scattering coefficient of the dermis was 200 cm^{-1}, 100 cm^{-1} for hypodermis, and 90 cm^{-1} for muscles. The anisotropy factor g for each layer was equal to 0.9. The selected values correspond to typical values of the absorption and scattering coefficients of the skin.[31] The thickness of the first layer, d_{dermis}, varied from 1 to 2.5 mm with a step of 0.5 mm. The values of thickness of the second layer $d_{\mathrm{hypodermis}}$ were 0.5, 1, 2, 3, 4, and 5 mm. The third layer (muscle) thickness was equal to 5 mm. As a result, 240,000 MCML simulations were performed with 10^7 photon packets each.

For intermediate values of the absorption and scattering coefficients, the values were interpolated between the grid nodes by the K-nearest neighbors method. The following normalization was carried out to select the neighboring absorption and scattering coefficients:

$$\mu_a^{\log} = \ln(\mu_a), \tag{3}$$

$$\mu_a^{\mathrm{norm}} = (\mu_a^{\log} - \min(\mu_a^{\log}))/(\max(\mu_a^{\log}) - \min(\mu_a^{\log})). \tag{4}$$

Hence, each normalized value of the absorption and scattering coefficient was uniformly distributed and varied from 0 to 1. As the input data for the interpolation model, the absorption coefficients μ_{a1}^{norm}, μ_{a2}^{norm}, and μ_{a3}^{norm}, the dermal thickness d_{dermis}, and the hypodermal thickness $d_{\mathrm{hypodermis}}$ were used. The target variable of the model was the reflectance $R(r)$ at a fixed distance. Based on the input parameters, the dataset was split into the training (95%) and test (5%) subsets. The optimal values for the number of neighbors were estimated using cross-validation on the training dataset.

The described approach made it possible to calculate the diffuse reflection spectra at different distances between the source and the detector for any combination of layers' thicknesses and absorbers concentrations using the spectral dependencies of their absorption and scattering coefficients. Next, the algorithms for determining water concentration, as well as the dermal thickness and hypodermal thickness, were developed.

2.5 *Simulation Configurations and Fitting*

The dataset containing simulated DRS spectra of three-layered structures was obtained using the described algorithm (Sec. 2.4). The volume fraction of water W in the upper layer varied in the range from 0.5 to 1, the thickness of the upper layer (dermis) d_{dermis} varied in the range from 1 to 2.5 mm, the thickness of the second layer (hypodermis) $d_{\mathrm{hypodermis}}$ varied in the range from 0.5 to 5 mm and the volume fat fraction F in the second layer (hypodermis) was fixed to 1. The volume of water fraction W_3 in the third layer (muscles) was fixed to 0.8.

Simulated DRS spectra for each distance r between the fibers were fitted by Eq. (2), and the dependences of the fitting parameters C_0, C_1, A_{water}, and A_{lipid} as a function of distance were obtained. Then, linear regressions for the fitting parameters against the input parameters were performed, and deviations of the predicted values from the true values were calculated. This approach allowed us to estimate the error of skin parameters determination obtained during the experiment. Two options were considered: (1) linear regression for the amplitudes at a single distance and (2) linear regression for all amplitudes at all source–detector separations.

The average relative error was calculated to assess the error of determining the input parameters from the linear regression for a single distance. The following calculations were carried out for the water volume fraction. For a distance r, the predicted water contribution W_{pred} was determined from the linear fit for A_{water}, and water content error $\delta_W(r)$ was calculated as

$$\delta_W(r) = \frac{1}{N}\sum_{i=0}^{N-1}\frac{|W_{pred}^{(i)}(r) - W^{(i)}|}{W^{(i)}}, \tag{5}$$

where the index i denotes various input parameter configurations (W, d_{dermis}, and $d_{\text{hypodermis}}$) and N is the number of these configurations. Similar calculations were made for the predicted values of dermal thickness d_{dermis} and hypodermal thickness $d_{\text{hypodermis}}$.

Dermal thickness and hypodermal thickness predictions were evaluated using both linear regression for A_{water} and A_{lipid} for a single distance and using general linear regression for A_{water} and A_{lipid} at all distances. Since these features are highly correlated and the machine learning procedure can lead to overfitting, the L2 regularization was carried out. After that, the model was trained on the spectra for a randomly sampled subset of input parameters, and the prediction error was evaluated on a test set that did not intersect with the training set.

2.6 *Experimental SR DRS Data Fitting*

The following approach was used for the interpretation of experimental diffuse reflectance spectra. US imaging allowed us to determine the thicknesses of the dermal and hypodermal layers while concentrations of molecular components in each layer remained unknown. Thus, linear regression between the amplitudes in Eq. (2) and the observed thicknesses was performed to analyze the possibility of experimental determination of the thickness from DRS data.

In the case of histamine-induced edema, when the dermal thickness was expected to vary, linear regression between A_{water} and US-determined dermal thickness was analyzed. In the second experiment, the normal skin of seven volunteers (two males, five females) was studied. The mean age of volunteers was 23 years, the minimum and maximum ages were 21 and 27, respectively. A model was built based on the linear regression with L2 regularization and leave-one-out validation. The A_{water} and A_{lipids} amplitudes obtained for all source-detector distances were used as predictive features.

3 Results and Discussion

3.1 *Assessment of the Cutaneous Edema in SR DRS*

The SR DRS technique was applied to assess variations in the skin parameters caused by edema induced by histamine application. Similar models for edema were used in previous works.[10,17]

Typical DRS spectra of the skin exhibit the bands centered at 930 nm (mainly originating from lipids in the hypodermis) and at 970 nm (water) [Fig. 3(a)]. Histamine application to the skin led to a pronounced increase of the 970-nm band, accompanied by a decrease of the 930-nm band [Fig. 3(b)].

The OD spectra were fitted in the 900- to 1075-nm range to characterize the contribution of lipids and water [Eq. (2), Fig. 3(c)]. Thus, amplitudes A_{water} and A_{lipid} as functions of distance between source and detection fibers were obtained [Fig. 3(d)]. To characterize the change in the water content of the dermis, the spectra measured at small distances between the fibers were analyzed. This configuration corresponds to shallow detection depth, which reduces the contribution of the hypodermis. The maximum increase of A_{water} during edema was $33 \pm 3\%$ relative to the control. However, based on the confocal Raman spectroscopy data,[32] the water content in the dermis can be estimated as ~70%. Hence, the 33% increase means water content rises to as much as ~90%. This value seems inadequate from the physiological point of view and, as shown below (Sec. 3.3), originates from the increase in dermal thickness.

The kinetics of the lipids absorption band A_{lipid} was estimated for the DRS measured at a distance of 10 mm when the detection depth is large and light reaches the hypodermis. A decrease in the A_{lipid} after edema induction was observed [Fig. 3(f)], which can be explained by the skin swelling and a concomitant decrease of the hypodermis contribution to the detection

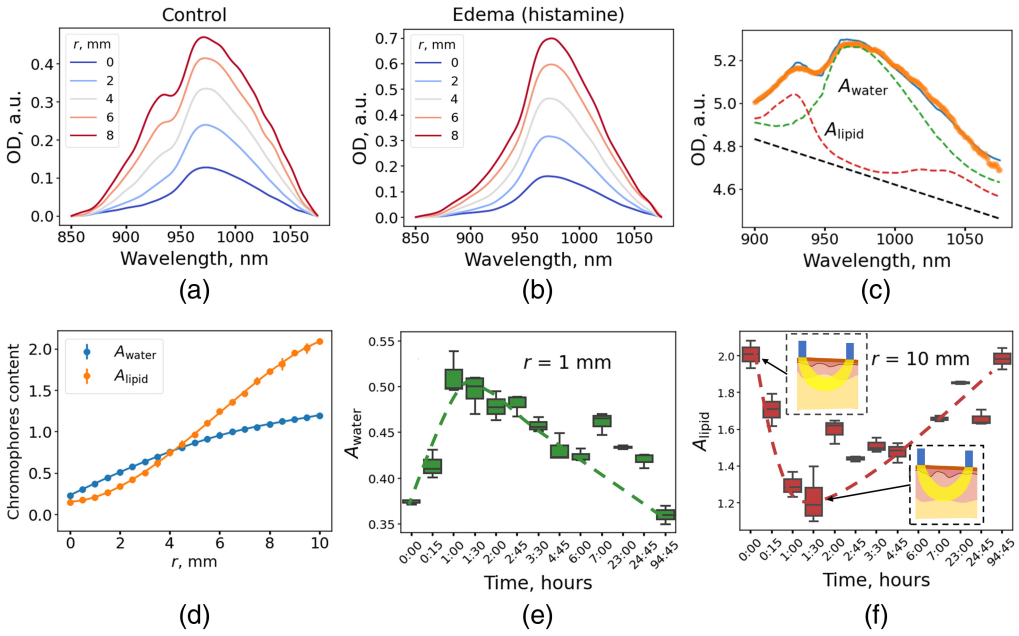

Fig. 3 Experimental OD spectra for normal skin (a) and following histamine application (b) measured in the same skin area. The parameter r denotes the source-detector separation in panels (a) and (b). (c) Example of fitting the measured DRS data with Eq. (2). Orange line corresponds to experimental data, blue line corresponds to fit, and green and red dashed lines corresponds to water and lipid contributions to the spectrum, respectively. (d) Representative dependence of the water and lipids amplitudes (A_{water} and A_{lipid}) on the distance between the source and the detector fibers. (e, f) Kinetics of the A_{water} (e) and A_{lipid} (f) amplitudes obtained for the $r = 1$ mm and $r = 10$ mm source-detector separation observed in the process of edema.

volume. The Monte-Carlo simulation of light propagation was performed to validate this hypothesis.

3.2 *SR DRS Modeling for Different Structures of the Skin*

Using the simulated SR DRS spectra of the three-layered skin model with varying parameters, we tested several approaches for the inverse problem solution, i.e., determination of (1) water content in the dermis, (2) dermal, and (3) hypodermal thickness.

The average simulated spectrum (denoted as OD) and the amplitude of the water-related component (denoted as A_{water}) and their standard deviation calculated for the set of models with a fixed water volume fraction of $W = 0.75$ and varying thickness of the dermis and hypodermis for source-detector distances of 1 and 10 mm are shown in Figs. 4(a) and 4(b), respectively. As shown, the standard deviation of the water absorption band is significantly higher for large source–detector separation.

Next, the water content error was estimated at a distance of 1 mm between the fibers. The relative error of 8.6% in determining the water content was at a distance between the fibers of 1 mm and increased with the source-detector distance. It can be assumed that A_{water} value is determined by both the water content in the dermis and dermis thickness at large distances between the fibers.

This suggestion is in agreement with the photon detection probability distribution [Fig. 4(c)], which allows estimating the fraction of detected photons from different depths. For typical system parameters ($W = 0.7$, $d_{dermis} = 1.5$ mm), calculations show that at a 1-mm source–detector separation, more than 80% of the signal is detected from the upper 1.1 mm of the skin. Since 80% of the response is formed in this layer, deeper layers do not make a significant contribution. Thus, with an increase in the dermal thickness above 1.1 mm, the response would not change significantly. On the contrary, with a change in water concentration in the dermis layer, one can expect a proportional increase in the peak of water absorption and amplitude A_{water}.

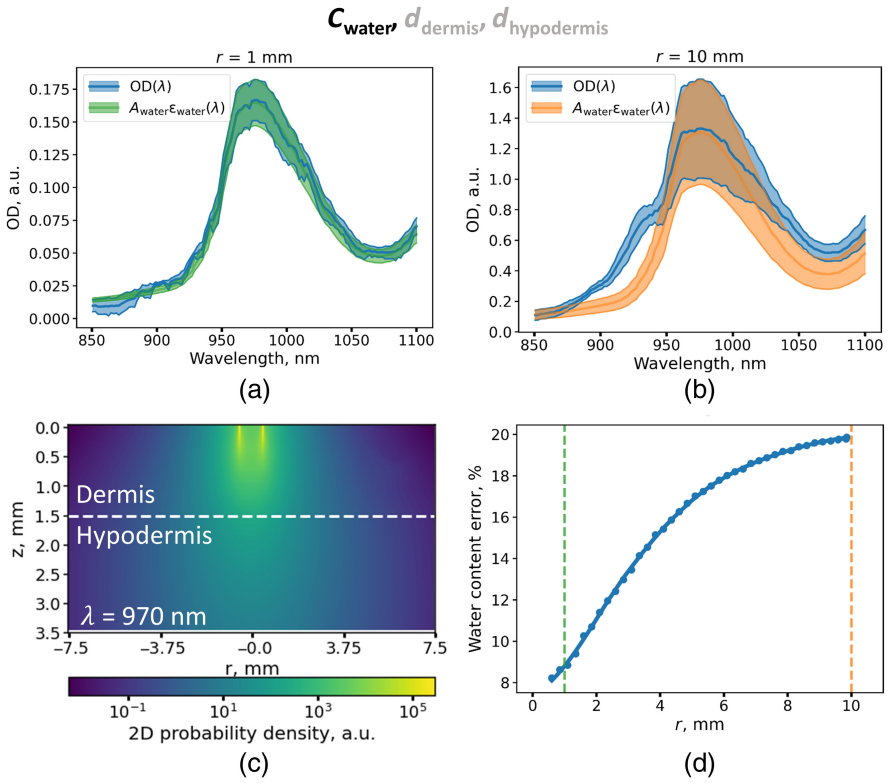

Fig. 4 Determination of water content c_{water} from simulated DRS for varying values of d_{dermis} and $d_{hypodermis}$. Average (blue line) and standard deviation (blue region) of the OD spectra sets for distance between the fibers of 1 mm (a) and 10 mm (b). The average spectrum and standard deviation of the water spectral contribution obtained from fitting of the spectra at distances between the fibers of 1 mm [panel (a), green] and 10 mm [panel (b), orange]. (c) Density probability distribution for photon detection at a distance between the source and the detector of 1 mm for a model with dermal water concentration $W = 0.75$ at a wavelength of 970 nm and with dermal thickness 1.5 mm. White dashed line corresponds to the border between dermis and hypodermis. (d) Average relative error of water concentration determined using the developed models as a function of the source–detector distance r. Each model uses data obtained at a single distance between the fibers.

Hence, it can be concluded that the amplitude A_{water} at small distances is mainly determined by the water content in the skin (see Figure S3 in the Supplementary Material).

The second parameter of interest was the thickness of the dermis, i.e., of the first layer in the MCML simulation. First, the error of determining the dermal thickness from the DRS spectra at a single distance between the source and the detector was assessed. As can be seen in Fig. 5(a), distance dependences of A_{water} for various dermal thicknesses differ significantly at large source-detector separation. The error in determining the thickness of the dermis $\delta_{dermis}(A_{water}; r)$ as a function of distance was calculated for this class of models and is represented in Fig. 5(c). As can be seen, the smallest error is achieved at 5 mm and is ~24%.

The smallest error of the dermal thickness determination using the A_{lipid} value $\delta_{dermis}(A_{lipid}; r)$ also demonstrated an error of about 19%. It was achieved for the interfiber distance of 2 mm [Fig. 5(c)]. To improve the accuracy of measuring the dermal thickness, a linear regression with the L_2 regularization that takes into account distance dependences of both A_{water} and A_{lipid} amplitudes was constructed, which yielded a 5% error of the dermal thickness determination [Fig. 5(d)].

Similar procedure was carried out for determination of the hypodermal thickness. The error was estimated for the models that take into account data for a single distance between the source and the detector. As can be seen in Fig. 6(a), distance dependences of A_{water} for various hypodermal thicknesses do not differ significantly. Therefore, using A_{water} to determine the thickness of the hypodermis results in a high measurement error (>80%) [Fig. 6(c)]. Substantial difference

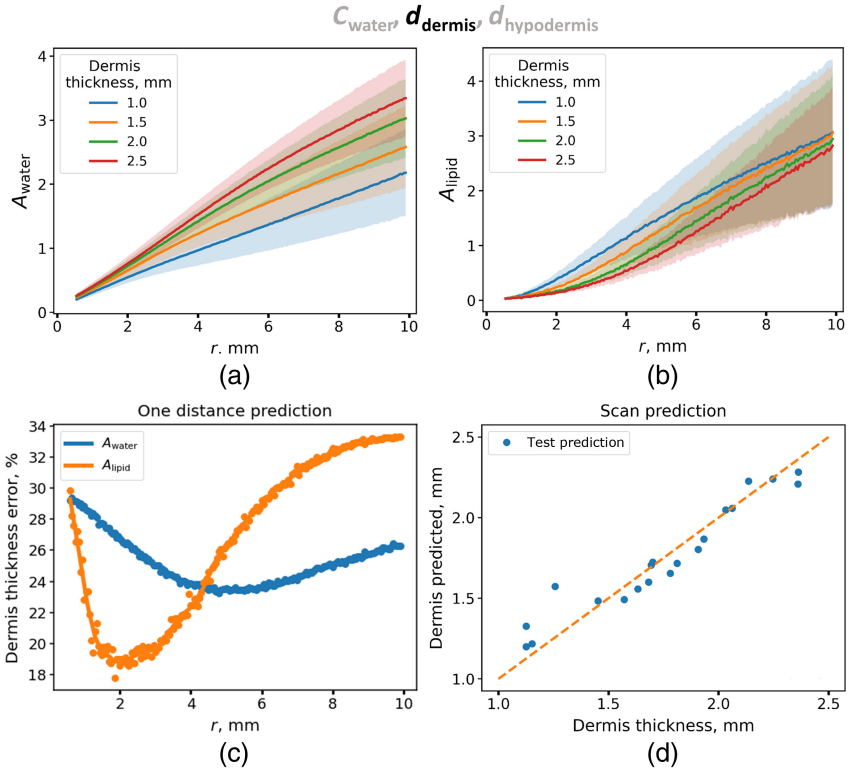

Fig. 5 (a) Dependences of the water absorption amplitude A_{water} on the distance between the source and the detector, obtained from the approximation of the calculated diffuse reflectance spectra for dermal thicknesses from 1 to 2.5 mm. (b) Dependences of the lipid absorption amplitude A_{lipid} on the distance between source and detector fibers, obtained from the approximation of the calculated diffuse reflectance spectra for dermal thicknesses from 1 to 2.5 mm. (c) Dependence of the error in the prediction of the thickness of the dermis from the absorption amplitude of water A_{water} (blue curve) and lipids A_{lipid} (orange curve) obtained at different distances between the source and the detector from the corresponding distance. (d) Scatter plot for true and predicted values of dermal thickness obtained on the test set using a linear regression model with L2 regularization.

in distance dependences of A_{lipid} at large distances leads to better results. The error $\delta_{hypodermis}$ (A_{lipid}; r) as a function of distance has a minimum of 13.4%, which is achieved for the interfiber distance of 10 mm [Fig. 6(c)]. Linear regression with the L_2 regularization that takes into account the whole set of distance dependences of the A_{water} and A_{lipid} amplitudes was built to predict hypodermal thickness. In Fig. 6(d), the dependence between the hypodermal thickness from the test set and the hypodermal thickness predicted using machine learning approach is presented. Machine learning approach allowed us to reduce the relative error of hypodermal thickness determination to 6.3%.

This simulation shows that the simultaneous use of parameters determined from SR DRS can significantly decrease the error of the dermal and hypodermal thickness determination. These considerations were further used for the analysis of the experimental data.

3.3 *Ultrasound Examination of the Skin Structure During Edema: Correlations with the SR DRS*

In addition to the SR DRS measurements presented in Fig. 3, a US study of cutaneous edema was performed to determine the thickness of the dermis. US images of the skin layers for the normal and edematous skin are shown in Figs. 7(a) and 7(b), respectively. Since the dermis and hypodermis have different acoustic properties, it is possible to discriminate between them in the US images.[33]

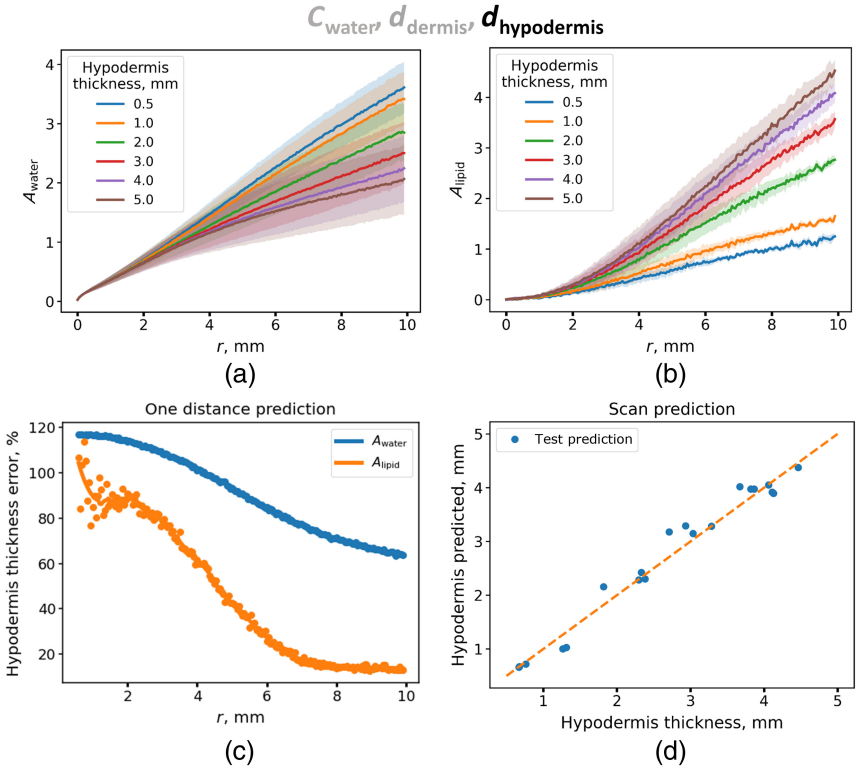

Fig. 6 (a) Water absorption amplitude A_{water} and (b) lipid absorption amplitude A_{lipid} as a function of the distance between the source and the detector for different hypodermal thicknesses. (c) Dependence of the error in the prediction of the thickness of the hypodermis from the absorption amplitude of water A_{water} (blue curve) and lipids A_{lipid} (orange curve) obtained at different distances between the source and the detector from the corresponding distance. (d) Scatter plot for true and predicted values of hypodermal thicknesses obtained on the test set using a linear regression model with L2 regularization.

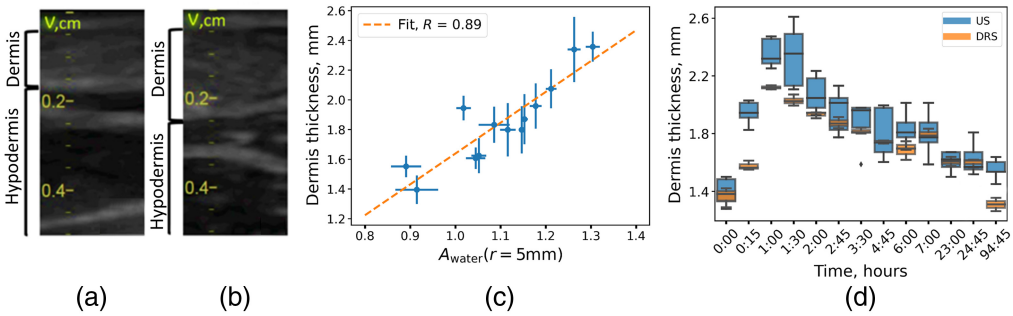

Fig. 7 The US images of skin structure for normal (a) and edematous skin (b). (c) Dependence of the US-measured dermal thickness on the amplitude of water absorption A_{water} obtained from the fitting of the diffuse reflectance spectra measured at a distance between the fibers of 10 mm. (d) Dermal thickness dynamics during edema determined by US and DRS (time axis is not to scale).

According to the US data, the thickness of the dermis increased from 1.4 to 2.2 mm during edema, that is consistent with the results from other studies.[34] Since for the simulation data the minimum of $\delta_{dermis}(A_{water}; r)$ was obtained at $r = 5$ mm [Fig. 5(c)], this approach was applied to the experimental SR DRS data. It was found that the Pearson correlation coefficient between the dermal thickness measured by US and determined from the A_{water} value was 0.89 [Fig. 7(c)]. The kinetics of the dermal thickness determined using the SR DRS and US upon histamine-induced edema are shown in Fig. 7(d).

It follows from the simulation data that the determination of water concentration from the A_{water} amplitude has an error of 8% associated with the variability of other parameters [Fig. 4(d)]. Considering the fact that the thickness of the dermis increased from 1.4 to 2.2 mm during edema, it is likely that this variation will influence the A_{water} value obtained at the minimum (1 mm) source–detector separation. From the data presented in Figs. 5(a) and S2, it can be deduced that such an increase is 15%. Thus, one can expect that out of a 33% increase in water contribution amplitude caused by edema [Fig. 3(e)], 15% is due to dermis swelling, and the rest is due to water content increase from 70% up to 81%. Hence, the correlation of the SR DRS parameters with dermal thickness has been demonstrated [Figs. 7(c) and 7(d)]. The observed dependence makes it possible to predict dermal thickness using experimental SR DRS data using measurements corresponding to higher values of interfiber distances. One of the limitations of the considered experiment is that it was performed for a single subject; therefore, we further evaluated the developed method by studying the skin parameters of healthy volunteers.

3.4 *Skin Structure Assessment Using SR DRS: From Dermis to Hypodermis*

US imaging and SR DRS measurements were performed for seven healthy volunteers. The measurements were carried out for different sites of the lower forearm: near the inner wrist, where the hypodermis layer is thin, near the antecubital fossa, where the hypodermis layer is thicker, and at the middle of the forearm. The thickness of the hypodermis, as determined from the US data, varied in the range of 0.5 to 4 mm for the tested subjects. The variability of the dermal thickness for volunteers was lower than for the case of edema. However, the thickness of the hypodermis layer observed in US images varied significantly.

To determine the thickness of the dermis from the SR DRS data, a model was built based on linear regression with L2 regularization. The A_{water} and A_{lipid} amplitudes obtained for all source-detector distances were used as the predictive features [Figs. 8(a) and 8(b)]. Dependence of

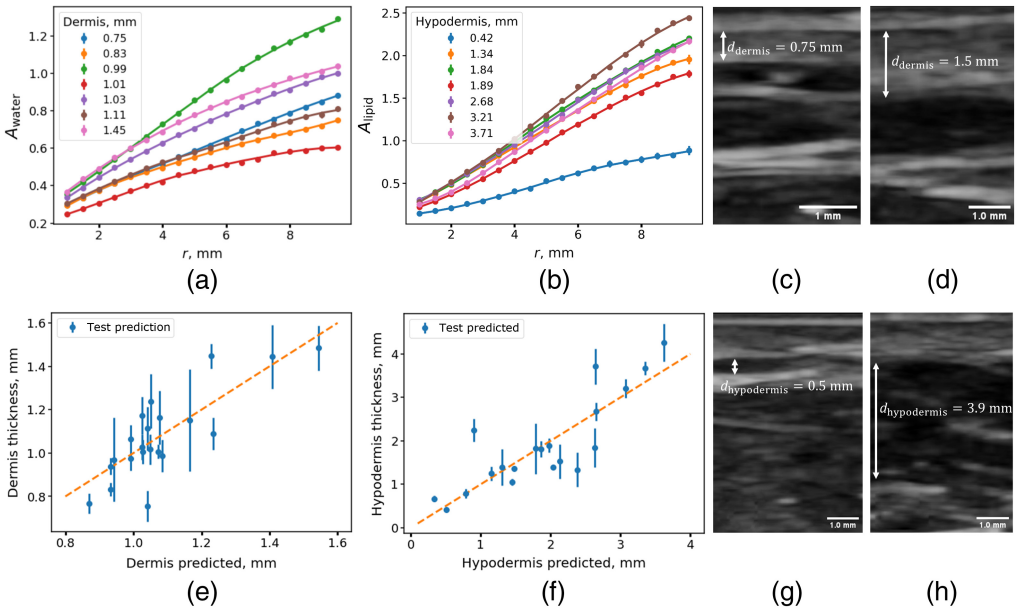

Fig. 8 (a) Dependences of the water absorption amplitude A_{water} on the distance between the source and the detector, obtained from the approximation of the diffuse reflectance spectra at different thicknesses of the dermis of volunteers. (b) Dependences of the lipid absorption amplitude A_{liid} on the distance between the source and the detector, obtained from the fitting of diffuse reflectance spectra for various values of hypodermal thickness. (c,d) US images corresponding to minimal and maximal dermal thicknesses. (e) Dependence of US-measured dermal thicknesses on those predicted using a model trained on water and lipids dependencies on interfiber distance. (f) Dependence of US measured hypodermal thicknesses on those predicted from lipids contribution measured at a distance between the fibers of 10 mm. (g,h) US images corresponding to minimal and maximal hypodermal thicknesses.

Table 1 Evaluation of models predicting physiological parameters of the skin using DRS data obtained in simulations and experimental measurements. The table represents RMSE and relative error of parameters, Pearson correlation coefficient R and p-value of non-correlation hypothesis for true and predicted values of parameters.

Parameters	RSME	Relative error (%)	R Pearson	p-value
		Simulation results		
C_{water}	0.08 mm	9.3	0.89	$\ll 5 \cdot 10^{-2}$
d_{dermis}	0.01 mm	5.0	0.97	$\ll 5 \cdot 10^{-2}$
$d_{hypodermis}$	0.02 mm	6.3	0.99	$\ll 5 \cdot 10^{-2}$
		Experimental results		
d_{dermis}	0.11 mm	8.3	0.82	$5 \cdot 10^{-6}$
$d_{hypodermis}$	0.56 mm	23.4	0.84	$3 \cdot 10^{-6}$

US-measured dermal thickness on predicted values is presented in Fig. 8(e). The true value was considered the value obtained using US. Using the predicted values according to Eq. (5), the average relative error was calculated.

As a result, the average relative error of the dermal thickness prediction was 8.3%. Next, we focused on searching spectral descriptors indicative of the hypodermal thickness in our data. For this purpose, the A_{lipid} amplitude at various distances between the source and detector fibers was estimated, and the dependence of the Pearson correlation coefficient between the thickness of the hypodermis and A_{lipid} was calculated. Evidently, at distances between the fibers larger than 2 mm, there was a high correlation (>0.8) between the thickness of the hypodermis and A_{lipids}, reaching the maximum of 0.87 at $r = 10$ mm (Figure S4 in the Supplementary Material). This result is in qualitative agreement with a result obtained for hypodermal thickness determination based on simulated data (Fig. 6). A linear regression was built to determine the thickness of the hypodermis from the experimental A_{lipids} amplitude obtained at a distance of 10 mm. The resulting model allowed the determination of the thickness of the hypodermis with an average relative error of 23.4% and an average root mean squared error (RMSE) of 0.56 mm [Fig. 8(f)].

4 Conclusion

In the present work, using the SR DRS technique, the possibility of determining the physiological parameters of the skin was investigated *in vivo* for a model of cutaneous edema and for the normal skin. The parameters of interest included (1) the concentration of water in the dermis, (2) dermal thickness, and (3) the thickness of the hypodermis.

The propagation of light in the skin was simulated using the Monte Carlo method. From the simulation data, spatially resolved diffuse reflectance spectra were calculated using machine learning methods. Based on the simulation data, approaches for determining the water content in the dermis and thickness of the hypodermis and dermis were developed. It was shown that the minimum relative error of 9.3% in determining the water concentration is achieved at a distance between the source and the detector equal to 1 mm. The lowest error of hypodermal thickness determination was achieved at a distance of 10 mm and was 13.4%.

The developed procedure yielded a 0.89 Pearson correlation coefficient between the dermal thickness measured by US examination and amplitude of water absorption obtained using SR DRS during edema. Finally, machine learning models were built to determine the thickness of dermis and hypodermis of normal skin *in vivo* using SR DRS and US data with a relative error of 8.3% and 23.4%, respectively (Table 1). Thus, the developed method allows for a

quantitative non-invasive relative assessment of molecular (water and lipids) and morphological (dermis and hypodermis thickness) parameters. Further development of this approach will be an important step in developing of a diagnostic method for assessing fluid retention in pathological conditions of heart failure and skin physiology for cosmetology and dermatology.

Disclosures

The authors state no conflict of interest.

Acknowledgments

The work was supported by the Russian Science Foundation (Grant No. 22-25-00864).

Code, Data, and Materials Availability

Data underlying the results presented in this paper are not publicly available at this time but may be obtained from the authors upon reasonable request.

References

1. P. Ponikowski et al., "2016 ESC Guidelines for the diagnosis and treatment of acute and chronic heart failure," *Eur. Heart J.* **37**(27), 2129–2200 (2016).
2. A. G. Smith et al., "Objective determination of peripheral edema in heart failure patients using short-wave infrared molecular chemical imaging," *J. Biomed. Opt.* **26**(10), 105002 (2021).
3. H. Wada et al., "Water and lipid content of breast tissue measured by six-wavelength time-domain diffuse optical spectroscopy," *J. Biomed. Opt.* **27**(10), 105002 (2022).
4. S. H. Chung et al., "Molecular imaging of water binding state and diffusion in breast cancer using diffuse optical spectroscopy and diffusion weighted MRI," *J. Biomed. Opt.* **17**(7), 071304 (2012).
5. A. E. Cerussi et al., "In vivo absorption, scattering, and physiologic properties of 58 malignant breast tumors determined by broadband diffuse optical spectroscopy," *J. Biomed. Opt.* **11**(4), 044005 (2006).
6. S. Verdier-Sévrain and F. Bonté, "Skin hydration: a review on its molecular mechanisms," *J. Cosmet. Dermatol.* **6**(2), 75–82 (2007).
7. M. Qassem and P. Kyriacou, "Review of modern techniques for the assessment of skin hydration," *Cosmetics* **6**(1), 19 (2019).
8. S. Jansen van Rensburg, A. Franken, and J. L. Du Plessis, "Measurement of transepidermal water loss, stratum corneum hydration and skin surface pH in occupational settings: a review," *Ski. Res. Technol.* **25**(5), 595–605 (2019).
9. G. S. Budylin et al., "In vivo sensing of cutaneous edema: a comparative study of diffuse reflectance, Raman spectroscopy and multispectral imaging," *J. Biophotonics* **15**(1), e202100268 (2022).
10. A. Y. Sdobnov et al., "Hydrogen bound water profiles in the skin influenced by optical clearing molecular agents—quantitative analysis using confocal Raman microscopy," *J. Biophotonics* **12**(5), e201800283 (2019).
11. X. Chen et al., "Exploiting complementary terahertz ellipsometry configurations to probe the hydration and cellular structure of skin in vivo," *Adv. Photonics Res.* **2**(1), 2000024, (2021).
12. F. Geldof et al., "Layer thickness prediction and tissue classification in two-layered tissue structures using diffuse reflectance spectroscopy," *Sci. Rep.* **12**, 1698 (2022).
13. B. Song et al., "Quantitative spatial mapping of tissue water and lipid content using spatial frequency domain imaging in the 900-to 1000-nm wavelength region," *J. Biomed. Opt.* **27**(10), 105005 (2022).
14. T. Nanjo et al., "Investigation of measurement area and source-detector distance in diffuse reflectance spectroscopy for leg edema induced by heart failure," *Proc. SPIE* **11968**, 119680C (2022).

15. G. N. Stamatas, M. Southall, and N. Kollias, "In vivo monitoring of cutaneous edema using spectral imaging in the visible and near infrared," *J. Invest. Dermatol.* **126**(8), 1753–1760 (2006).
16. Y. Shimojo et al., "Measurement of absorption and reduced scattering coefficients in Asian human epidermis, dermis, and subcutaneous fat tissues in the 400- to 1100-nm wavelength range for optical penetration depth and energy deposition analysis," *J. Biomed. Opt.* **25**(4), 045002 (2020).
17. Y. Wang et al., "Three-dimensional histological structures of the human dermis," *Tissue Eng. Part C Methods* **21**(9), 932–944 (2015).
18. M. Arrigo et al., "Acute heart failure," *Nat. Rev. Dis. Prim.* **6**(1), 16 (2020).
19. V. V Tuchin, "*Handbook of Optical Biomedical Diagnostics*, SPIE Press, Bellingham, Washington (2002).
20. X. Zhong, X. Wen, and D. Zhu, "Lookup-table-based inverse model for human skin reflectance spectroscopy: two-layered Monte Carlo simulations and experiments," *Opt. Express* **22**(2), 1852–1864 (2014).
21. M. Sharma et al., "Verification of a two-layer inverse Monte Carlo absorption model using multiple source-detector separation diffuse reflectance spectroscopy," *Biomed. Opt. Express* **5**(1), 40–53 (2014).
22. Y.-W. Chen and S.-H. Tseng, "Efficient construction of robust artificial neural networks for accurate determination of superficial sample optical properties," *Biomed. Opt. Express* **6**(3), 747 (2015).
23. S.-Y. Tsui et al., "Modelling spatially-resolved diffuse reflectance spectra of a multi-layered skin model by artificial neural networks trained with Monte Carlo simulations," *Biomed. Opt. Express* **9**(4), 1531–1544 (2018).
24. M. Ivančič et al., "Efficient estimation of subdiffusive optical parameters in real time from spatially resolved reflectance by artificial neural networks," *Opt. Lett.* **43**(12), 2901–2904 (2018).
25. P. S. Rudraiah, H. Duadi, and D. Fixler, "Extraction of optical properties from a turbid medium using fiber probe for spectral and spatial diffuse reflectance measurement," *OSA Contin.* **4**(2), 762–773 (2021).
26. P. S. Rudraiah, H. Duadi, and D. Fixler, "Bottom layer absorption coefficients extraction from two-layer phantoms based on crossover point in diffuse reflectance," *J. Biomed. Opt.* **26**(11), 117001 (2021).
27. C. Eisenbeiss et al., "Evaluation of blood oxygen saturation in vivo from diffuse reflectance spectra," *J. Biomed. Opt.* **6**(4), 457–467 (2001).
28. N. R. Rovnyagina et al., "Grading cartilage damage with diffuse reflectance spectroscopy: optical markers and mechanical properties," *J. Biophotonics* **16**, e202200149 (2022).
29. C. A. Schneider, W. S. Rasband, and K. W. Eliceiri, "NIH Image to ImageJ: 25 years of image analysis," *Nat. Methods* **9**(7), 671–675 (2012).
30. E. Alerstam et al., "Next-generation acceleration and code optimization for light transport in turbid media using GPUs," *Biomed. Opt. Express* **1**(2), 658–675 (2010).
31. S. L. Jacques, "Optical properties of biological tissues: a review," *Phys. Med. Biol.* **58**(11), R37 (2013).
32. C. A. Téllez-Soto et al., "In vivo determination of dermal water content in chronological skin aging by confocal Raman spectroscopy," *Vib. Spectrosc.* **112**, 103196 (2021).
33. L. Tognetti et al., "Dermoscopy: fundamentals and technology advances," in *Technology in Practical Dermatology*, M. Fimiani, P. Rubegni, and E. Cinotti, Eds., pp. 3–24, Springer, Cham (2020).
34. C. Eisenbeiss et al., "Influence of body water distribution on skin thickness: measurements using high-frequency ultrasound," *Br. J. Dermatol.* **144**(5), 947–951 (2001).

Biographies of the authors are not available.